On the ISAR Image Analysis and Recovery with Unavailable or Heavily Corrupted Data

Ljubiša Stanković, *Fellow IEEE*

[1] ***Abstract*—Common ISAR radar images and signals can be reconstructed from much fewer samples than the sampling theorem requires since they are usually sparse. Unavailable randomly positioned samples can result from heavily corrupted parts of the signal. Since these samples can be omitted and declared as unavailable, the application of the compressive sensing methods in the recovery of heavily corrupted signal and radar images is possible. A simple direct method for the recovery of unavailable signal samples and the calculation of the restored ISAR image is reviewed. An analysis of the noise influence is performed. For fast maneuvering ISAR targets the sparsity property is lost since the ISAR image is blurred. A nonparametric quadratic time-frequency representations based method is used to restore the ISAR image sparsity. However, the linear relation between the signal and the sparsity domain transformation is lost. A recently proposed gradient recovery algorithm is adapted for this kind of analysis. It does not require a linear relation of the signal and its sparsity domain transformation in the process of unavailable data recovery. The presented methods and results are tested on several examples proving the expected accuracy and improvements.**

***Keywords*: Radar imaging, ISAR, time-frequency analysis, noisy signal, sparse signal, compressive sensing.**

I. Introduction

In inverse synthetic aperture radar (ISAR) a high resolution image of a target is obtained by using the two-dimensional Fourier transform (FT) of received (and processed) signal. The ISAR image of a point target is a highly concentrated two-dimensional point spread function whose position corresponds to the target's range and cross-range. For a number of scattering points, the radar image consists of several peaks at the range and cross-range positions [1]-[6]. Usually the number (area) of nonzero values in the ISAR image is small as compared to the total number of signal samples. Thus, we may say that a common signal in ISAR is sparse in the two-dimensional Fourier domain. As such it can be reconstructed from much fewer samples than the sampling theorem requires. Unavailable, randomly positioned samples could also result from heavily corrupted parts of the signal, that are omitted and declared as unavailable, before the ISAR image recovery and calculation is done. Measurements and physical constraints of the target and radar interferences may also cause that only some of the randomly positioned data can be received and measured. The fact that the two-dimensional FT domain is the domain of the ISAR signal sparsity is used in signal recovery. This fact allows application of the compressive sensing (CS) methods [7]-[17] in the ISAR imaging [2],[18]-[24]. A simple method for the unavailable radar data recovery and the ISAR image calculation is reviewed in the paper. This method belongs to the class of the orthogonal matching pursuit recovery CS methods, [9]-[13]. An analysis of the noise influence on this radar image is done. A simple and accurate relation for the output signal-to-noise ratio is derived.

For fast maneuvering ISAR targets, radar image can be spread over the two-dimensional FT domain [1], [5], [25]-[28]. Then a large number of the two-dimensional FT values are nonzero, covering a significant part of the radar image. In this case the sparsity property of the signal is lost. One possibility to restore this property is to use parametric transforms to compensate and refocus the ISAR image, making it sparse again [1], [25], [28]-[33]. However, a large number of parameters should be used for almost each scattering point in the case of a general nonuniform motion. Good results can be achieved using these techniques, but at the expense of a high computational load. This kind of parametric calculation is even more complex for the reduced set of available signal samples, when the CS methods are going to be used. Another way to refocus the image is based on the quadratic time-frequency representations [1], [31], [34], [35]. A representation which can achieve high concentration, like in the Wigner distribution case, at the same time avoiding the cross-terms, is the S-method, [31], [36], [37]. This method is nonparametric and computationally quite simple. It requires just a few additions and multiplications on the already calculated ISAR image using the two-dimensional FT. However, the S-method relation to the signal is not linear. Therefore, many conventional CS based recovery techniques, including the one reviewed in this paper, can not be used. They are based on the direct linear reconstruction relation between the signal and the transform in the domain of signal sparsity. This is not the case in the quadratic signal representations. It was the reason why the recently proposed method for recovery of missing samples/measurements [17] is adapted for the problem formulation in this paper. This method belongs to the class of gradient methods [16]. Its application does not require a direct linear relation of the signal to its sparsity transformation domain in the process of recovery of unavailable signal values.

The presented methods and results are illustrated and tested on several examples proving the expected efficiency.

The manuscript is organized as follows. A brief review of the signal model in the considered ISAR systems is given in Section II. A reconstruction algorithm for the radar signal

Electrical Engineering Department, University of Montenegro, 20000 Podgorica, Montenegro, email: ljubisa@ac.me, www.tfsa.ac.me. This research is supported by the Ministry of Science project CS-ICT (Grant No. 01-1002).

with unavailable data is presented in Section III, along with the analysis of noise influence in Section IV. The gradient method for the reconstruction of the ISAR images, corresponding to nonuniform motion is presented in Section V. Examples illustrate the accuracy of the proposed methods.

II. Radar Signal Model

Consider a linear frequency-modulated continuous-wave (FM-CW) radar. Assume that it transmits signal in a form of series of M chirps [38]. The received signal (scattered from a target) is delayed with respect to the transmitted signal for $t_d(t) = 2d(t)/c$, where $d(t)$ is the target distance from the radar and c is the speed of light. A deramping-based architecture is assumed, with a replica of the transmitted signal being mixed with the returned echoes. The received signal, after an appropriate demodulation, compensation, and residual video phase filtering, is

$$q(m,t) = \sigma e^{j\Omega_0 \frac{2d(t)}{c}} e^{-j2\pi B f_r (t-mT_r)\frac{2d(t)}{c}} \tag{1}$$

where σ is the reflection coefficient of the target, while Ω_0 is the radar operating angular frequency. The repetition time of a single chirp is denoted by $T_r = 1/f_r$, while the number of samples within each chirp is N. The coherent integration time (CIT) is $T_c = MT_r$. Index m corresponds to the chirp index (slow time). The received signal for a system of point scatterers can be modeled as a sum of the individual point scatterer responses, [1]. The Doppler part in the received signal of a point target is

$$s(t) = \sigma e^{j2d(t)\Omega_0/c}. \tag{2}$$

The range part of the received signal $\exp(-j2\pi B f_r(t - mT_r)2d(t)/c)$ reduces to $\exp(j2\pi\gamma n/N)$ with $\gamma = -Bf_rT_sN(2d(t)/c)$ and $t - mT_r = nT_s$. The sampling interval within a chirp is denoted by $T_s = T_r/N$ and n is the index of signal sample within one chirp (fast-time). The two-dimensional FT of the discrete received and processed signal $q(m,n)$ is

$$Q(k,l) = \sum_{m=0}^{M-1}\sum_{n=0}^{N-1} q(m,n) e^{-j(\frac{2\pi mk}{M} + \frac{2\pi nl}{N})}, \tag{3}$$

where the indices k and l are the discrete two-dimensional FT frequencies. They are proportional to the cross-range and range respectively. Illustration of the discrete values of $q(m,n)$ within one revisit is presented in Fig. 1.

For a target which consists of K scattering points, the resulting signal can be written as

$$q(m,t) = \sum_{i=1}^{K} \sigma_i e^{j\Omega_0 \frac{2d_i(t)}{c}} e^{-j2\pi B f_r (t-mT_r)\frac{2d_i(t)}{c}}$$

where σ_i is the reflection coefficient of the ith scattering point and $d_i(t)$ is its distance to radar.

III. Uniform Target Motion with Unavailable/Corrupted Data

In the simplest case, when the target motion may be considered as uniform within the CIT, the distance of the ith scattering point to radar can be written as

$$d_i(t) \cong d_0 + v_i t \cong d_0 + v_i m T_r.$$

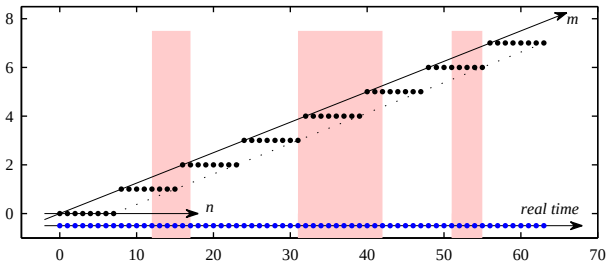

Fig. 1. Illustration of one revisit (chirp series) discretization in coordinates m (chirp index, slow time) and n (time within one chirp, fast time), along with a real time. The case of $M = 8$ chirps in one revisit and $N = 8$ samples within chirp is presented. The CIT is 64 samples. Unavailable or heavily corrupted data are marked by red.

Since the distance between the radar and target is large, then $d_i(t) = \sqrt{(d_0 + x_i(t))^2 + y_i^2(t)} \cong (d_0 + x_i(t))$, where $x_i(t)$ and $y_i(t)$ are the range and cross-range coordinates of the ith scattering point with respect to the center of target (on the line-of-sight). The range coordinate $x_i(t)$ is related to its original position (x_{i0}, y_{i0}) by a rotation transform $x_i(t) = x_{i0}\cos(\omega_R t) + y_{i0}\sin(\omega_R t) \cong x_{i0} + y_{i0}\omega_R t$. After distance compensation all changes in the distance $d_i(t)$ reduce to the movements along the line-of-sight, defined by $x_i(t)$. A method for distance compensation in the case of reduced set of data is presented in [2].

The received signal, from the ith scattering point, after the distance compensation, is

$$\begin{aligned} q_i(m,n) &= \sigma_i e^{j\Omega_0 2v_i T_r m/c} e^{j2\pi\gamma_i n/N} \\ &= \sigma_i e^{j2\pi\beta_i m/M} e^{j2\pi\gamma_i n/N}, \end{aligned}$$

where $v_i = y_{i0}\omega_R$, $\beta_i = 2\Omega_0 y_{i0}\omega_R T_r/c$ and $\gamma_i = -Bf_rT_sN(2d_i(t)/c)$ are the constants proportional to the velocity (cross-range y_{i0}) and range (after distance d_0 compensation $\gamma_i = -2Bx_{0i}/c$ since $T_s = T_r/N = 1/(f_rN)$). The total signal for K scattering points is

$$q(m,n) = \textstyle\sum_{i=1}^{K} q_i(m,n).$$

Assume that some samples or blocks of samples of the received radar signal are either unavailable or heavily corrupted so that they are omitted from the analysis [15]. Assume that the blocks of omitted signal samples are randomly positioned. The two-dimensional FT of this signal is then

$$\hat{Q}(k,l) = \sum_{m=0}^{M-1}\sum_{n\in\mathbb{N}_A(m)} q(m,n) e^{-j(\frac{2\pi mk}{M} + \frac{2\pi nl}{N})}. \tag{4}$$

It can happen that the unavailable/corrupted data are: all within one chirp or spread over two or more chirps, including the possibility that a few chirps in a row are affected in this way, Fig. 1. These cases are included by using the notation $n \in \mathbb{N}_A(m)$ where $\mathbb{N}_A(m)$ is the set of available samples within the mth chirp. For some m it could also happen that $\mathbb{N}_A(m) = \varnothing$, i.e., that there are no available samples within that chirp. The total number of available samples is $1 \ll N_A \leq MN$. Consider one scattering point and two cases [27]:

(1) For $k=\beta_i$ and $l=\gamma_i$ we will have

$$\hat{Q}(k,l)=\sum_{m=0}^{M-1}\sum_{n\in\mathbb{N}_A(m)}\sigma_i=\sigma_i N_A \tag{5}$$

where N_A is the total number of available samples.

(2) For $k\neq\beta_i$ or $l\neq\gamma_i$ we have

$$\hat{Q}(k,l)=\sum_{m=0}^{M-1}\sum_{n\in\mathbb{N}_A(m)}\sigma_i e^{j\phi_i(n,m,k,l)}=\Xi_i(k,l). \tag{6}$$

The variable $\Xi_i(k,l)$ defined by (6) can be considered as random since the positions of N_A terms used in the second summation are random, for $n\in\mathbb{N}_A(m)$ and $\phi_i(n,m,k,l)=(2\pi m(k-\beta_i)/M+2\pi n(l-\gamma_i)/N)$. For a large number of randomly positioned unavailable samples $1\ll N_A\ll NM$ the value of $\Xi_i(k,l)$ is a sum of vectors with quasi arbitrary phases. It can be considered as a complex-valued variable (missing samples noise) with Gaussian distributed real and imaginary parts (as shown in [40]). Its variance is

$$\mathrm{var}\{\hat{Q}(k,l)\}=N_A\frac{NM-N_A}{NM-1}\sigma_i^2. \tag{7}$$

Therefore, for K scattering points we may write [40]

$$\mathrm{E}\{\hat{Q}(k,l)\}=\sum_{i=1}^{K}\sigma_i N_A\delta(k-\beta_i,l-\gamma_i) \tag{8}$$

$$\mathrm{var}\{\hat{Q}(k,l)\}=N_A\frac{NM-N_A}{NM-1}\sum_{i=1}^{K}\sigma_i^2\left(1-\delta(k-\beta_i,l-\gamma_i)\right).$$

A. Reconstruction Algorithm

For a sufficiently small ratio ρ of the standard deviation coefficient (7) and a component mean value $\sigma_i N_A$

$$\rho=\sqrt{\frac{NM-N_A}{N_A(NM-1)}} \tag{9}$$

correct detection of the signal component positions is achieved [40]. This ratio, with a clear probabilistic meaning, is the (Welch) bound for the coherence index $\mu\geq\rho$ of matrix with available samples, used to define the reconstruction condition bound within the spark framework [2]. The number of components K can be easily included for the worst case of approximately equal values of σ_i. Then $K(NM-N_A)/[N_A(NM-1)]$ should be sufficiently small [40], [41]. When these conditions are satisfied the received signal and the ISAR image recovery can be done using the following simple and computationally efficient algorithm.

Algorithm:

(i) Calculate the initial transform estimate $\hat{Q}(k,l)$ by using the available/remaining signal values and (4) or in matrix form

$$\hat{\mathbf{Q}}=\mathbf{\Phi y}, \tag{10}$$

where $\mathbf{y}$ is the vector of available samples $q(m,n)$, $n\in\mathbb{N}_A(m)$

$$\mathbf{y}=[q(m,n)\,|\;\; n\in\mathbb{N}_A(m)]^T.$$

Note that the two-dimensional data $q(n,m)$ are transformed into a column vector $\mathbf{y}$ and Φ is the corresponding transformation matrix. It is used to produce $\hat{Q}(k,l)$ arranged into a column vector $\hat{Q}$.

(ii) Set the resulting transform values $Q(k,l)$ to zero at all positions (k_i,l_i) except the highest $\hat{K}$ values in the initial estimate $\hat{Q}(k,l)$, i.e.,

$$\begin{aligned}&Q(k,l)=0\;\;\text{for}\;(k,l)\neq(k_i,l_i),\;i=1,2,...,\hat{K}\\&(k_i,l_i)=\underset{i=1,2,...,\hat{K}}{\arg}\{\max\{\mathrm{sort}\{|Q(k,l)|\}\}\}.\end{aligned} \tag{11}$$

This criterion is not sensitive to the assumed number of nonzero coefficients $\hat{K}$ as far as all nonzero positions of the original transform are detected and the total number $\hat{K}$ of transform values in $\hat{Q}(k,l)$ is lower than the number of available samples, i.e., $K\leq\hat{K}\leq N_A$. All $\hat{K}-K$ transform values that are zero in the original signal will be found as zero-valued in the algorithm.

(iii) The unknown $\hat{K}$ transform coefficients could be then easily calculated by solving the set of N_A equations for available instants $n\in\mathbb{N}_A(m)$, at the detected nonzero candidate positions (k_i,l_i), $i=1,2,...,\hat{K}$. The linear system for unknowns $Q(k_i,l_i)$ is obtained using the inverse two-dimensional FT for N_A available signal values,

$$\begin{aligned}&\frac{1}{MN}\textstyle\sum_{i=1}^{\hat{K}}Q_{\hat{K}}(k_i,l_i)e^{j(\frac{2\pi mk_i}{M}+\frac{2\pi nl_i}{N})}=q(m,n),\\&\text{for}\;0\leq m\leq N-1,\quad n\in\mathbb{N}_A(m).\end{aligned} \tag{12}$$

System (12) is a system of N_A linear equations with only $\hat{K}$ unknown transform values $Q(k_i,l_i)$ denoted by $Q_{\hat{K}}(k_i,l_i)$. This linear system can be written in a matrix form as

$$\mathbf{\Psi Q}_{\hat{K}}=\mathbf{y}, \tag{13}$$

where: $\mathbf{Q}_{\hat{K}}$ is a vector whose elements are unknowns $Q(k_i,l_i)$, $i=1,2,...,\hat{K}$, $\mathbf{\Psi}$ is the corresponding coefficients matrix, and $\mathbf{y}$ is a vector whose elements are available signal $q(m,n)$ samples. In general, for $\hat{K}<N_A$ the system is solved in the least square sense as

$$\mathbf{Q}_{\hat{K}}=\left(\mathbf{\Psi}^H\mathbf{\Psi}\right)^{-1}\mathbf{\Psi}^H\mathbf{y}. \tag{14}$$

where H denotes the Hermitian transpose operation. The reconstructed coefficients $Q(k_i,l_i)$, $i=1,2,...,\hat{K}$, (vector $\mathbf{Q}_{\hat{K}}$) are equal to the transform coefficients of the original signal for all detected candidate frequencies. If some transform coefficients, whose true value should be zero, are included (when $K<\hat{K}$) the resulting system will produce their correct (zero) values [41].

The condition that the system (12), with $\hat{K}$ unknowns, has a unique solution is that there are at least $\hat{K}$ independent equations, i.e., that $\mathrm{rank}(\mathbf{\Psi})\geq\hat{K}$. Note that this unique solution, in theory does not exclude possibility that another set of $\mathbf{Q}_{\hat{K}}$ may exist satisfying the same set of available samples. This will be commented later. If system (12) has the solution and all true nonzero coefficient $Q(k,l)$ positions are included based on estimate (4) and (11) and the ratio (9) is sufficiently small (including K) then the recovery in this sense is achieved. The fact that all signal components are

included can be easily checked after the calculation is done, by calculating the mean squared error between the reconstructed samples and the available samples, at the positions of the available samples $n \in \mathbb{N}_A(m)$

$$MSE = \frac{1}{N_A} \sum_{m=0}^{M-1} \sum_{n \in \mathbb{N}_A(m)} |q(m,n) - q_R(m,n)|^2 , \quad (15)$$

where

$$q_R(m,n) = \frac{1}{MN} \sum_{k=0}^{M-1} \sum_{l=0}^{N-1} Q_R(k,l) e^{j(\frac{2\pi mk}{M} + \frac{2\pi nl}{N})}$$

and $Q_R(k,l)$ are the reconstructed coefficients. The full set of reconstructed coefficients consists of the set of zero-valued coefficients $Q_R(k,l) = 0$ for $(k,l) \neq (k_i, l_i)$, $i = 1, 2, ..., \hat{K}$ (according to (11)) and the reconstructed values of non-zero candidate coefficients $Q_R(k,l) = Q_{\hat{K}}(k,l)$ for $(k,l) = (k_i, l_i)$, $i = 1, 2, ..., \hat{K}$ (according to (12)).

Comments:

Large $\hat{K}$, close to N_A, will increase the probability that the signal recovery is achieved in one step. However, for large $\hat{K}$ computational complexity is increased. In the case of additional input noise in available samples, a value of $\hat{K}$ as close to the true signal sparsity K as possible will reduce the noise influence on the reconstructed signal. This will be shown later. If the algorithm fails to detect all components with initially assumed $\hat{K}$ (the reconstruction accuracy of the available samples defined by (15) can be used to detect this event) the procedure should be repeated after the detected components are reconstructed and removed. In such cases the iterative procedure should be used.

In theory, after the zero MSE is achieved and a sparse solution, satisfying the available samples is obtained, check of its uniqueness should be done. In simulation it is done by calculating the MSE over all signal samples after the reconstruction. The restricted isometry property (RIP) [14] defines the condition that the resulting reconstruction of a specific signal from the reduced set of samples is unique. However, its practical application is not computationally feasible. After (12) is solved and K nonzero values $Q(k_i, l_i)$ are found satisfying $MSE = 0$ this analysis would require a combinatorial check if any other set of K (or less) nonzero valued $Q(k,l)$ can produce the same result for given $\mathbf{y}$. Another approach to check the uniqueness of the obtained solution is based on the spark and coherence index analysis [2]. These results are pessimistic for applications since they include zero probability events. The spark based relation would be obtained within the presented framework if we assume that the missing sample noises of different scattering points of the same (unity) reflection coefficients σ_i are added up in (6) with the same phase to produce $\Xi_i(k,l)K$ at some point (k,l). Variable $\Xi_i(k,l)$ should also assume its maximal possible value denoted by $\mu N_A = \max_{i,k,l} \{|\Xi_i(k,l)|\}$ (calculated over all possible (β_i, γ_i) and all possible positions (k,l))[2]. It should also be assumed that $(K-1)$ remaining missing sample noise components at the component position (β_i, γ_i) assume the same maximal value μN_A and that all of them subtract in phase from the signal mean value N_A at (β_i, γ_i). Condition for correct detection of a component at (β_i, γ_i) is then $N_A - N_A\mu(K-1) > N_A\mu K$ or $K < \frac{1}{2}(1 + 1/\mu)$. This is a quite pessimistic bound for K since it uses the worst case value $\max_{i,k,l} \{\Xi_i(k,l)\}$ of any possible signal in a calculation for a specific signal. Its also assumes that all noise components are added up (or subtracted) in phase as well as that the component amplitudes σ_i are the same. Therefore, for a high degree of randomness, a probabilistic approach indicated at the beginning of this subsection may be more suitable for the analysis [40], [41]. A posteriori check of the solution uniqueness can also be done [43].

[2]Equality $\mu N_A = |\Xi_i(k,l)|$ holds for all i, k, l for matrices of very specific structure called complex equiangular tight frames [44]. Even in that case the phase of various $\Xi_i(k,l)$ is not the same and for a large number of signal components with different phases the probabilistic approach would be suitable.

Iterative procedure:

If the signal contains components with significantly different amplitudes, ratio (9) can be small only with respect to the largest components. Lower amplitude components can not be initially detected. Then the iterative procedure should be used. Algorithm for the iterative procedure is:

-The largest component at (k_1, l_1) in (4) is detected. The transform values $Q(k,l)$ are set to zero at all positions (k,l) except at the position of the highest one at (k_1, l_1). This component is reconstructed using (12) with $\hat{K} = 1$ and subtracted from the signal.

-The remaining signal is used to calculate (4) again. The highest value position (k_2, l_2) is found, and signal is reconstructed at two frequency points $\{(k_1, l_1), (k_2, l_2)\}$ using (12) with $\hat{K} = 2$. The reconstructed signal is removed from the original signal and (4) is calculated with the remaining signal.

-Procedure is continued in this way until the reconstruction accuracy of the available samples is bellow the required accuracy level. The accuracy is defined with (15) as difference of $\hat{K}$ components at positions $\{(k_1, l_1), (k_2, l_2), ..., (k_{\hat{K}}, l_{\hat{K}})\}$, and the given available signal values $n \in \mathbb{N}_A(m)$.

-Number of iterations in this procedure can be significantly reduced if we combine it with the first approach by grouping, for example, $\hat{K} = 3$ or $\hat{K} = 4$ components of similar amplitudes in each step.

Example 1: A signal with $K = 16$ randomly positioned scattering points

$$q(m,n) = \textstyle\sum_{i=1}^{16} \sigma_i e^{j2\pi\beta_i m/M} e^{j2\pi\gamma_i n/N},$$

with $M = N = 64$ is considered with 87.5% unavailable samples. A set of random positive values of scattering coefficients σ_i is taken. A half of the random amplitudes ($K/2 = 8$) is taken to produce the resulting ISAR image values around 0 [dB] range, while a half of the random scattering coefficients are reduced to a level of about -40 [dB] range. The two-dimensional FT (ISAR image) of the original signal, if all signal samples were available, is presented in Fig.2(a). The initial two-dimensional FT of the signal is calculated using (4) with $N_A = 0.125MN$ available samples, Fig.2(b). It is presented in Fig.2(c). The largest $\hat{K} = 10$ values in $\hat{Q}(k,l)$ are taken as candidates for the nonzero coefficients. In this step small signal components were masked by the noise from large values (described by (6)). Therefore the reconstruction

of small components is done using the procedure (12)-(14). The reconstructed signal is subtracted from the original signal and the procedure is repeated. The result from this iterative procedure is presented in Fig.2(d). The difference between the available signal values and the reconstructed signal values, at the same positions, is within the computer precision. This difference (measured by (15)) is used as the stopping criterion. Check of the solution is done after reconstruction as well, by calculating the MSE over all signal samples, to exclude the possibility that the reconstructed signal is equal to the original one at the available signal sample positions only.

The recovery is also tested using various numbers of the scattering points K and various numbers of available samples N_A. In this case the stopping criterion was also the MSE value at the positions of the available samples. Statistical results are obtained by averaging over 100 independent realizations with random scattering coefficients, frequency positions, and positions of the available samples, Fig.3. We can conclude that the number of scattering points which can be recovered in this case, with a high probability, using N_A randomly positioned signal values is of an order of $K \sim N_A/5$, corresponding to $K(NM - N_A)/[N_A(NM - 1)] < 1/5$.

From Fig.3 it is obvious that, for a given number of available samples, for example, $N_A = 256$, the MSE is at the computer precision level in all 100 realizations for the number of components below $K = 48$. Also there was no successful reconstruction for $K > 100$. Between these two values, for signals with a number of components $50 < K < 100$, obviously there were some reconstruction and some non-reconstruction realizations.

IV. Influence of Additive Input Noise

Assume now that an input additive noise $\varepsilon(n)$ exists in the available data. Note that the noise due to missing values influences the results in the sense presented in the previous section. When the recovery is achieved accuracy of the result is related to the input additive noise in signal samples. It depends on the number of available signal samples and nonzero transform coefficients (sparsity) as it will be shown next. The reconstruction equations (12) for noisy available data are

$$q(m,n) + \varepsilon(m,n) = \frac{1}{MN}\sum_{i=1}^{\hat{K}} Q_{\hat{K}}(k_i,l_i) e^{j(\frac{2\pi m k_i}{M} + \frac{2\pi n l_i}{N})}, \quad (16)$$

$$\text{for } 0 \le m \le N-1, \quad n \in \mathbb{N}_A(m).$$

The transform indices can take a value from the set of detected values $(k,l) \in \{(k_1,l_1),(k_2,l_2),...,(k_{\hat{K}},l_{\hat{K}})\}$. A matrix form of equations (16) is

$$\mathbf{y} + \boldsymbol{\varepsilon} = \boldsymbol{\Psi}\mathbf{Q}_{\hat{K}}.$$

This is a system of N_A linear equations with $\hat{K}$ unknowns $Q_{\hat{K}}(k_i,l_i)$ in vector $\mathbf{Q}_{\hat{K}}$. The solution is

$$\boldsymbol{\Psi}^H(\mathbf{y}+\boldsymbol{\varepsilon}) = \boldsymbol{\Psi}^H\boldsymbol{\Psi}\mathbf{Q}_{\hat{K}}$$
$$\mathbf{Q}_{\hat{K}} = \left(\boldsymbol{\Psi}^H\boldsymbol{\Psi}\right)^{-1}\boldsymbol{\Psi}^H(\mathbf{y}+\boldsymbol{\varepsilon})$$
$$\mathbf{Q}_{\hat{K}} = \mathbf{Q}_{KS} + \mathbf{Q}_{KN}. \quad (17)$$

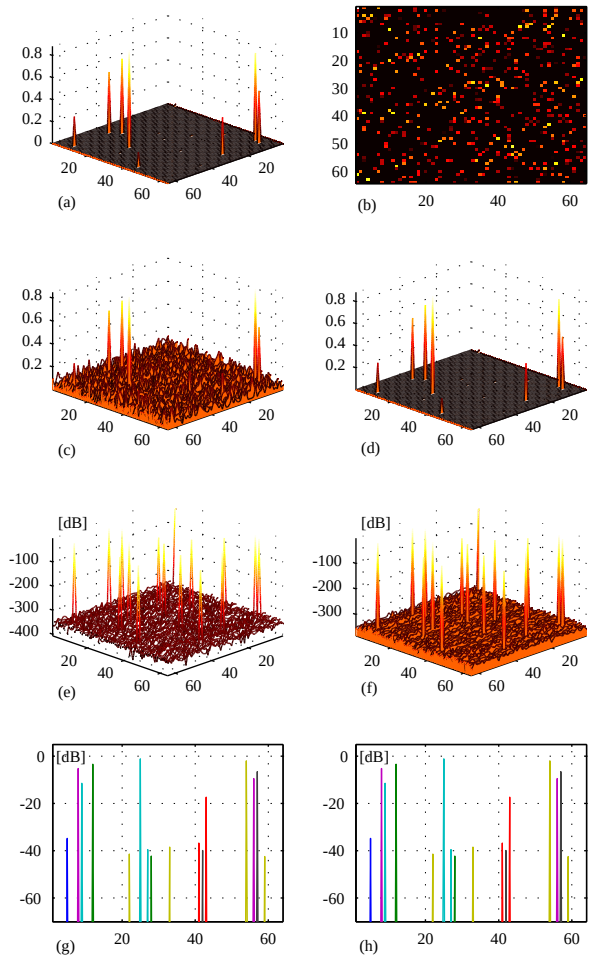

Fig. 2. (a) A two-dimensional Fourier transform of the considered radar signal (ISAR image). (b) Radar signal with 12.5% of available/uncorrupted samples (unavailable/corrupted samples are presented in black). (c) The two-dimensional Fourier transform calculated using the available samples of the radar signal. (d) The reconstructed ISAR image. (e) A two-dimensional Fourier transform of the considered radar signal (ISAR image) in logarithmic scale. (f) The reconstructed ISAR image in logarithmic scale. (g)-(h) Graphs from (e)-(f), respectively, from the zero-angles view to compare the amplitudes in logarithmic scale.

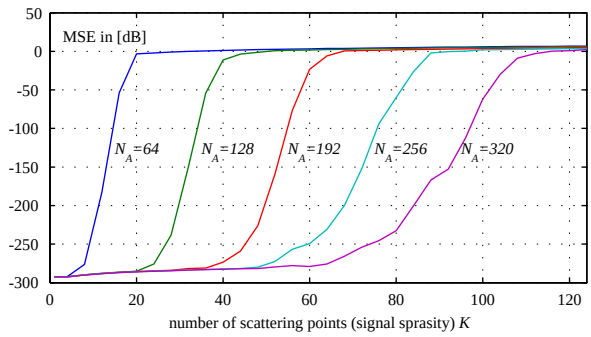

Fig. 3. Full recovery performance of the algorithm as function of the number of scattering points K for some numbers of available samples N_A. Statistical results are obtained by averaging over 100 independent realizations with random signal amplitudes, frequency positions, and positions of available samples.

The true transform coefficients and the noise influence to the reconstructed transform are

$$\mathbf{Q}_{KS} = \left(\mathbf{\Psi}^H\mathbf{\Psi}\right)^{-1}\mathbf{\Psi}^H\mathbf{y},$$
$$\mathbf{Q}_{KN} = \left(\mathbf{\Psi}^H\mathbf{\Psi}\right)^{-1}\mathbf{\Psi}^H\boldsymbol{\varepsilon}.$$

If all signal samples were available, the input signal-to-noise (SNR) ratio, would be

$$SNR_i = 10\log\frac{\sum_{m=0}^{M-1}\sum_{n=0}^{N-1}|q(m,n)|^2}{\sum_{m=0}^{M-1}\sum_{n=0}^{N-1}|\varepsilon(m,n)|^2} = 10\log\frac{E_s}{E_\varepsilon}. \tag{18}$$

Assume that the noise energy in the available samples is

$$E_{\varepsilon A} = \sum_{m=0}^{M-1}\sum_{n\in\mathbb{N}_A(m)}|\varepsilon(m,n)|^2. \tag{19}$$

The true scattering coefficient (component amplitude) in the signal transform at the position (k_i, l_i), in the case if all signal samples were used, would be $MN\sigma_i$. To compensate the resulting transform for the known bias in amplitude (5) when only N_A available samples are used, the coefficient should be multiplied by MN/N_A. In a full recovery, a signal transform coefficient is equal to the coefficient of the original signal with all signal samples being used. The noise in the transform coefficients is multiplied by the same factor of MN/N_A. Therefore, the energy of noise in the reconstruction algorithm is increased to $E_{\varepsilon A}(MN/N_A)^2$. The SNR in the fully recovered signal is

$$SNR_f = 10\log\frac{\sum_{m=0}^{M-1}\sum_{n=0}^{N-1}|q(m,n)|^2}{\frac{M^2N^2}{N_A^2}\sum_{m=0}^{M-1}\sum_{n\in\mathbb{N}_A(m)}|\varepsilon(m,n)|^2} \tag{20}$$

Since only $\hat{K}$ out of MN coefficients are used in the reconstruction the energy of the reconstruction error is reduced for the factor of $\hat{K}/(MN)$ as well. The energy of noise in the recovered signal is

$$E_{\varepsilon R} = \frac{\hat{K}}{MN}\frac{M^2N^2}{N_A^2}\sum_{m=0}^{M-1}\sum_{n\in\mathbb{N}_A(m)}|\varepsilon(m,n)|^2.$$

The SNR in the recovered signal is

$$SNR = 10\log\frac{\sum_{m=0}^{M-1}\sum_{n=0}^{N-1}|q(m,n)|^2}{\frac{\hat{K}NM}{N_A^2}\sum_{m=0}^{M-1}\sum_{n\in\mathbb{N}_A}|\varepsilon(m,n)|^2}. \tag{21}$$

Since the variances of noise in all samples and the available samples are the same then

$$\frac{1}{N_A}\sum_{m=0}^{M-1}\sum_{n\in\mathbb{N}_A(m)}|\varepsilon(m,n)|^2 = \frac{1}{MN}\sum_{m=0}^{M-1}\sum_{n=0}^{N-1}|\varepsilon(m,n)|^2 \tag{22}$$

Thus, the SNR in the recovered signal, according to (21), (22) and (18), is

$$SNR = SNR_i - 10\log\left(\frac{\hat{K}}{N_A}\right). \tag{23}$$

We may conclude that in the case of additive input noise in the available signal samples, the output SNR will be increased if the number $\hat{K}$ is as small as possible, for a given number of available samples N_A. In an ideal case, with respect to the additive noise, value of $\hat{K}$ should be equal to the signal sparsity $\hat{K} = K$.

Example 2: Consider a noisy signal from Example 1 with $K = 10$ signal components. Assume that an additive complex-valued Gaussian noise exists, with the input SNR equal to

$$SNR_i = 9.05 \text{ [dB]}$$

and $N_A = MN/8$. Since $K = 10$ in the previous example we used estimated value $\hat{K} = 14$ for the calculation. According to (23) the output SNR is

$$SNR = SNR_i - 10\log\left(\hat{K}/N_A\right)$$
$$= 9.05 + 15.81 = 24.86 \text{ [dB]}.$$

The improvement in SNR is 15.81 [dB]. This result is statistically checked. The statistical result is obtained by averaging over 100 realizations with random scattering coefficients and positions. The obtained statistical value of the output SNR is

$$SNR^{(stat)} = 24.53 \text{ [dB]}.$$

Agreement with the theory is almost exact, within the statistical confidence for the number of performed realizations.

If the number of components were estimated exactly as $\hat{K} = 10$, then the SNR values would be obtained as

$$SNR = 26.32 \text{ [dB]}$$
$$SNR^{(stat)} = 26.26 \text{ [dB]}.$$

The SNR value for $\hat{K} = 10$ would be higher for $10\log(14/10) = 1.46$ [dB] than in the case with $\hat{K} = 14$. In the iterative realizations, the case of $\hat{K} = 14$ would occur if there were 4 false detected components (maxima) before the signal reconstruction is achieved.

V. Nonuniform Target Motion

For fast moving targets and complex motions, the target over all M chirps, in one revisit, cannot be considered as the one with constant velocity motion. Then a higher-order approximation of the ith scattering point distance

$$d_i(t) \cong d_0 + v_{0i}t + a_it^2/2 + \ldots,$$

should be used with $v_i(t) = v_{0i} + a_it + \ldots$. If we assume that $v_i(t) = v_{0i} + a_it$, then the Doppler shift is a linear function of time. Its rate is a_i. Instead of a delta pulse concentrated at one frequency, corresponding to v_{0i}, we will obtain a FT of a linear frequency-modulated signal (or higher-order frequency-modulated signal), whose instantaneous frequency changes are proportional to the velocity $v_i(t)$ changes. The radar image, based on this form, is centered at the same position as the FT image, but with the spreading term in the cross-range (Doppler) direction of the form $\exp\left(j\frac{2\Omega_0}{c}(\frac{1}{2!}d_i''(0)t^2 + ...)\right)$ due to the target motion. The discrete domain signal is [31]

$$q_i(m,n) = \sigma_i e^{j2\pi\beta_i m/M}e^{j\alpha_i m^2/2+\ldots}e^{j2\pi\gamma_i n/N},$$
$$Q_i(k,l) = (2\pi)^2\sigma_i\delta(k-\beta_i, l-\gamma_i) *_k \mathrm{FT}\{e^{j\alpha_i m^2/2+\ldots}\}$$

where $\alpha_i = 2\Omega_0 T_r^2 d_i''(0)/c$ and $*_k$ is the convolution in the discrete cross-range domain, while $\delta(k,l) = 1$ for $k = l = 0$

and $\delta(k,l) = 0$ elsewhere. This spread can be significant and the resulting ISAR image is not sparse or sparsity is significantly degraded.

If the two-dimensional FT is corrected according to the S-method [31], [36], [37], along the cross-range direction, then the resulting image will be

$$SM_i(k,l) = (2\pi)^2 \sigma_i^2 \delta(k-\beta_i, l-\gamma_i).$$

It is sparse again and does not depend on $d_i''(0)$. Under certain conditions this representation is free of cross-terms among different scattering points, producing

$$SM(k,l) = (2\pi)^2 \sum_{i=1}^{K} \sigma_i^2 \delta(k-\beta_i, l-\gamma_i).$$

As in the most of the literature, it has been assumed that the range migrations are not significant as compared to the Doppler migrations. The range migrations are related to much smaller time interval than the Doppler migrations. Thus, a quadratic phase along the Doppler axis only are considered. In the case that the range migration should be taken into account [39], then an additional application of the presented method to the range direction is straightforward by using two-dimensional S-method (SM). It has been done in [31].

The S-method based ISAR image can be easily realized in a recursive way starting from

$$SM_0(k,l) = |Q(k,l)|^2, \tag{24}$$

with $SM_0(k)$ being the standard two-dimensional FT based radar image. The S-method based presentation can be achieved starting with the already obtained FT-based radar image $Q(k,l)$, with an additional simple calculation according to

$$SM_L(k,l) = SM_{L-1}(k,l) + 2\,\mathrm{Re}\{Q(k+L,l)Q^*(k-L,l)\}$$

or

$$\mathrm{SM}_L[q(m,n)] = SM_L(k,l) \tag{25}$$
$$= |Q(k,l)|^2 + 2\sum_{z=1}^{L} \mathrm{Re}\{Q(k+z,l)Q^*(k-z,l)\}.$$

The signal sampling interval in the S-method is the same as in the FT [36].

In this way, using the S-method, we will restore signal sparsity in the ISAR image domain. However we have lost the possibility to use a direct linear relation between the signal and the sparsity domain transformation. For a reduced set of $N_A < MN$ available signal samples, $n \in \mathbb{N}_A(m)$ the problem statement is now

$$\min \|SM_L(k,l)\|_0 \text{ subject to unchanged values in } \mathbf{y}. \tag{26}$$

where $\mathbf{y}$ is the vector of the available signal samples $q(m,n)$, $n \in \mathbb{N}_A(m)$ and $\|SM_L(k,l)\|_0$ is the number of nonzero values in $SM_L(k,l)$. The simple counting of nonzero coefficients by using the zero-norm is, in theory, the best optimization function. Finding the unavailable signal value to produce the minimal number of nonzero coefficients in the resulting presentation is an obvious optimization criterion. However, this criterion is very sensitive to small values in $SM_L(k,l)$. Also the gradient solutions are not possible with the zero-norm functions, since they are completely flat for any nonoptimal value. Thus only combinatorial approach could used. It is NP hard and computationally not feasible problem. That is why the norm-one is used in the standard CS methods instead of the norm-zero. In the S-method formulation the norm which will correspond to the commonly used norm-one of the FT is

$$\min \|SM_L(k,l)\|_{1/2} \text{ subject to unchanged values in } \mathbf{y}. \tag{27}$$

with

$$\|SM_L(k,l)\|_{1/2} = \textstyle\sum_{k=0}^{N-1}\sum_{l=0}^{N-1} |SM_L(k,l)|^{1/2}.$$

This form for $L = 0$ reduces to the norm-one of the FT, since

$$\sum_{k=0}^{N-1}\sum_{l=0}^{N-1} |SM_0(k,l)|^{1/2} = \sum_{k=0}^{N-1}\sum_{l=0}^{N-1} |Q(k,l)| = \|Q(k,l)\|_1$$

Minimization of $\sum_{k=0}^{N-1}\sum_{l=0}^{N-1} |SM_L(k,l)|^{1/2}$ has already been used for the time-frequency optimization in [42]. It is known that, under certain conditions, the norm-one produces the same result as the norm-zero in the problem formulation (26) for the cases when signal transformation is linear (for $L = 0$), [7], [8]. A simple gradient algorithm to iteratively calculate the missing signal values, while keeping available samples $q(m,n)$ unchanged, [17], is adapted for the problem formulation (27). It is presented next.

A. Gradient Algorithm

This gradient algorithm is inspired by the adaptive signal processing methods with an adaptive step size. It is a gradient descent algorithm where the missing samples are corrected according to the gradient of the sparsity measure corresponding to norm-one. The missing values converge to the point of a minimal sparsity measure of the signal representation. In common CS algorithms the signal coefficients in the domain of sparsity are the reconstruction goal. In this algorithm the missing samples/measurements are the reconstruction aim.

The algorithm for missing samples reconstruction is implemented as follows:

Step 0: Set $s = 0$, $p = 0$ and form the initial signal $y^{(0)}(m,n)$ defined for all m and n as:

$$y^{(0)}(m,n) = \begin{cases} q(m,n) & \text{for available samples, } n \in \mathbb{N}_A(m) \\ 0 & \text{for } n \notin \mathbb{N}_A(m) \end{cases},$$

The initial value for an algorithm parameter Δ is estimated as

$$\Delta = \max_{n \in \mathbb{N}_A(m)} |q(m,n)|. \tag{28}$$

Step 1: Set $y_r(m,n) = y^{(p)}(m,n)$. This signal is used in Step 3 in order to estimate reconstruction precision.
Step 2.1: Set $p = p+1$. For each missing sample at (n_i, m_i) for $n \notin \mathbb{N}_A(m)$ form the signals $y_1(m,n)$ and $y_2(m,n)$:

$$y_1(m,n) = y^{(p)}(m,n) + \Delta\delta(n-n_i, m-m_i)$$
$$y_2(m,n) = y^{(p)}(m,n) - \Delta\delta(n-n_i, m-m_i). \tag{29}$$

Step 2.2: Estimate differential of the signal transform measure denoted by $\mathcal{M}\{T[y_i(m,n)]\}$

$$g(m_i,n_i)=\frac{\mathcal{M}\{T[y_1(m,n)]\}-\mathcal{M}\{T[y_2(m,n)]\}}{N} \quad (30)$$

where in our case $\mathcal{M}\{T[y_i(m,n)]\}=\|SM_{i,L}(k,l)\|_{1/2}$ and $SM_{i,L}(k,l)=SM_L[y_i(m,n)]$ are the S-methods of $y_1(m,n)$ and $y_2(m,n)$, respectively, calculated with L correction terms. If the DFT of signal were the sparsity domain we would use $\mathcal{M}\{T[y_i(m,n)]\}=\|DFT_i(k,l)\|_1$, [45].

Step 2.3: Form a gradient matrix $\mathbf{G}_p$ with the same size as the signal $q(m,n)$. At the positions of available samples $n\in\mathbb{N}_A(m)$, this matrix has the value $G_p(m,n)=0$. At the positions of missing samples $n_i\notin\mathbb{N}_A(m)$ its values are $G_p(m,n)=g(m_i,n_i)$, calculated by (30).

Step 2.4: Correct the values of $y(m,n)$ iteratively by

$$y^{(p)}(m,n)=y^{(p-1)}(m,n)-G_p(m,n), \quad (31)$$

Step 3: If the maximal allowed number of iterations $P_{\max}$ is reached stop the algorithm. Otherwise calculate

$$T_{rsh}=\frac{\sum_{m=0}^{M-1}\sum_{n\notin\mathbb{N}_A(m)}|y_r(m,n)-y^{(p)}(m,n)|^2}{\sum_{m=0}^{M-1}\sum_{n\notin\mathbb{N}_A(m)}|y^{(p)}(m,n)|^2}.$$

Value of T_{rsh} is an estimate of the reconstruction error to signal ratio, calculated for missing samples only. If T_{rsh} is above the required precision threshold (for example, if $T_{rsh}>0.001$), the calculation procedure should be repeated with smaller Δ. For example, set new Δ value as $\Delta/\sqrt{10}$, increment the step counter $s=s+1$, and go to Step 1.

Step 4: Reconstruction with the required precision is obtained in p iterations or when the maximal allowed number of iterations $P_{\max}$ is reached. The reconstructed signal is $q_R(m,n)=y(m,n)=y^{(p)}(m,n)$.

Comments on the algorithm:

- Inputs to the algorithm are the signal size $M\times N$, set of available signal samples N_A, available signal values $q(m_i,n_i)$, $n_i\in\mathbb{N}_A(m)$, the maximal allowed number of iterations $P_{\max}$ and the required precision used in Step 3. The algorithm output is the reconstructed signal matrix $q_R(m,n)=y(m,n)$. If the input signal is complex-valued then the real and imaginary parts of signal samples are changed independently.

- The gradient algorithm using the norm-one and a large number of variables (missing signal values), as approaching to the optimal point, will produce a solution close to the exact signal samples, with a precision related to the algorithm step Δ. The precision is improved by using adaptive step Δ. A value of Δ equal to the signal magnitude (28) is used in the starting iteration. When the optimal point is reached then the algorithm will not improve the reconstruction precision any more, for a given algorithm step Δ. When this case (in Step 3) is detected the step Δ is reduced, and the same calculation procedure is continued from the reached reconstructed signal values. In several steps, the algorithm can approach the true signal values with a required precision. By performing presented iterative procedure, if there is a sufficient number of available samples, it is expected that the missing values will converge to the true signal values, producing the minimal sparsity measure in the ISAR image domain, [17],[43].

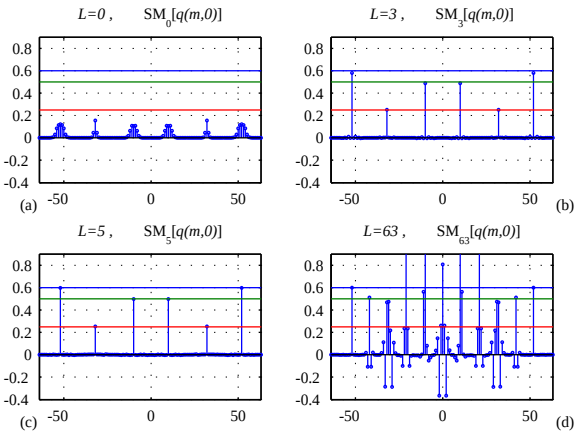

Fig. 4. All signal samples (chirps) available: (a) The Fourier transform based presentation. (b) The S-method with three correction terms, $L=3$. (c) The S-method with five correction terms, $L=5$. (d) The Wigner distribution based presentation (the S-method with $L=63$). Horizontal lines (red, green, blue) present the level of the true squared amplitudes of the components.

Example 3: A signal corresponding to the Doppler part of a radar signal is considered first. Its form is

$$\begin{aligned}q(m,0)&=\sum_{i=1}^{6}\sigma_i e^{j2\pi\beta_i m/M}e^{j\alpha_i m^2/2}\\&=2\sqrt{0.6}\cos(52m\pi/64-2.2\pi(m/64)^2)\\&+2\sqrt{1/2}\cos(10m\pi/64+2\pi(m/64)^2)\\&+2\sqrt{1/4}\cos(32\pi m/64-0.75\pi(m/64)^2)\end{aligned}$$

with $-64\le m\le 63$ and $\sigma_i\in\{\sqrt{0.6},\ \sqrt{0.6},\ \sqrt{0.5},\ \sqrt{0.5},\ \sqrt{0.25},\ \sqrt{0.25}\}$, $\beta_i\in\{26,\ -26,\ 5,\ -5,\ 16,\ -16\}$ and $\alpha_i\in\{-1.1\pi/1024,\ 1.1\pi/1024,\ \pi/1024,\ -\pi/1024,\ -0.375\pi/1024,\ 0.375\pi/1024\}$, for $i=1,2,...,6$. The representations with all available samples are presented in Fig.4. The FT based presentation (radar image) is shown in Fig.4(a) for $L=0$ since $SM_0(k,0)=|Q(k,0)|^2$. We can see that although there are just 6 scattering points the number of nonzero (significant) values in $SM_0(k)$ is above 40. The sparsity condition is heavily degraded. Adding just a few of the correction terms, according to (25), and calculating the S-method based presentation the sparsity in ISAR image is restored. Presentations with $L=3$ and $L=5$ in the S-method are shown in Fig.4(b)-(c). Note that the Wigner distribution, $WD(k,0)=SM_{63}(k,0)$, although well concentrated for the components, can not be used due to emphatic cross-terms which degrade the sparsity, Fig.4(d).

Consider next the same signal with 45 missing signal values (missing chirps). Here, the S-method is calculated with $L=5$ and the gradient based reconstructed algorithm is applied. The S-method, assuming all missing values are set to 0, is presented in Fig.5(a) for the initial iteration. The next iteration steps according to the presented iterative algorithm (denoted by step counter s), improve the presentation toward the case as if all data were available, Fig.5(b)-(d) for $s=2,4,$ and 16.

Example 4: A simulated setup is considered using radar operating at the frequency $f_0=10.1\,GHz$, $\Omega_0=2\pi f_0$, band-

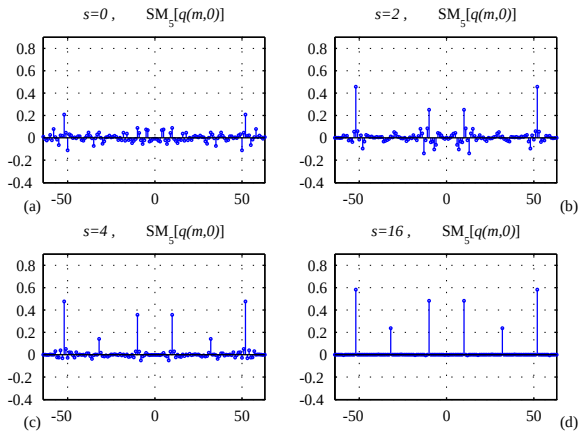

Fig. 5. The S-method presentation (radar image) with missing/corrupted 1/3 of the signal samples (chirps): (a) Initial S-method presentation $s = 0$, and the reconstructed S-method in the next iterations (b)-(d) with $s = 2$, $s = 4$, and $s = 16$, respectively.

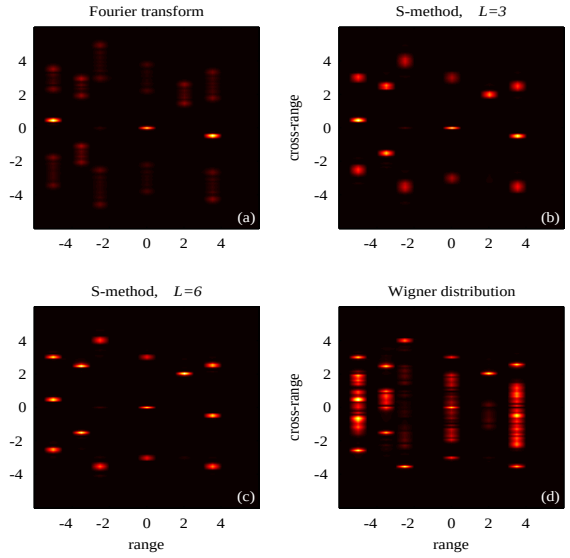

Fig. 6. The ISAR image based on: (a) The two-dimensional Fourier transform. (b) The S-method with $L = 3$. (c) The S-method with $L = 6$. (d) The Wigner distribution (the S-method with $L = 64$). All data are available.

width of linear frequency-modulated chirps $B = 300\,\text{MHz}$, and the coherent integration time $T_c = 2\,\text{s}$. The pulse repetition time is $T_r = T_c/256$ with the sampling interval $T_s = T_r/64$. The target is at 2 km distance from the radar, and rotates at $\Omega_R = 4\pi/180\,\text{rad/s} = 4\,^{\circ}\text{/s}$. The nonlinear rotation with frequency $\Omega = \pi\,\text{rad/s}$ is superimposed, $\Omega_R(t) = \Omega_R + A\sin(\Omega t)$, and amplitude $A = 1.25\pi/180\,\text{rad/s}$ corresponds to the total change in angular frequency Ω_R for $2.5\pi/180\,\text{rad/s}$. Note that here the range and the cross-range resolutions are $R_{\text{range}} = c/(2B) = 0.5\,\text{m}$, and $R_{\text{cross-range}} = \pi c/(\Omega_0 T_c \Omega_R) = 0.106\,\text{m}$ (calculated for $T_c = 2\,\text{s}$ with $\Omega_R \cong 4\pi/180\,\text{rad/s}$, neglecting effects of the nonlinear rotation). It has been assumed that there are 16 scattering points at the positions $(x_i, y_i) \in \{(-5,-2.5),(-5,0.5),(-5,3),(-3.5,-1.5),(-3.5,2.5),(-2.5,-3),(-2.5,0),(-2.5,4),(0,-3),(0,0),(0,3),(2,-3),(2,2),(3.5,-3.5),(3.5,-0.5),(3.5,2.5)\}$. The scattering coefficients of 14 scattering points are of order 1, while 2 scattering points, at $(-2.5,0)$ and $(2,-3)$, are with scattering coefficients lower for an order of -12 [dB] than the rest of points. First, the case with all available data is considered. The ISAR image based on the two-dimensional FT is presented in Fig.6(a). The S-method based ISAR image with $L = 3$ and $L = 6$ is shown in in Fig.6(b)-(c). It can be seen that just a few correction terms to the FT based ISAR image significantly improve the concentration. The Wigner distribution (the S-method with $L = 64$) is highly concentrated. However it suffers from the cross-terms, Fig.6(d). The range and cross-range coordinate axes are scaled with the resolution parameters to present range and cross-range in meters. The nonuniform motion could be reduced by reducing the CIT. This kind of reduction would also lead to a reduced resolution $R_{\text{cross-range}}$. In our example the total number of cross range bins is already too small that this approach could be used.

The case with 50% of the data being unavailable (or removed due heavy corruption) is considered next. The ISAR image calculated by using the two-dimensional FT is presented in Fig.7(a). As we can see the image sparsity is low. Since a large amount of the data is missing this image can not be improved by a direct application of the S-method since the missing data behave as a noise (Section II.A). The S-method based image with $L = 6$ is shown in Fig.7(b). The same holds for the Wigner distribution (the S-method with $L = 64$) given in Fig.7(c). However, the original image calculated with the S-method is highly sparse. Therefore the unavailable data can be reconstructed by minimizing the S-method subject to the available data, equation (27). The gradient based method is used to solve this minimization problem. The reconstructed S-method is almost the same as the S-method of the signal with all available data. It is presented in Fig.7(d). Two scattering points with small coefficients are hardly visible in 7(d). In order to provide their visible presentation 14 stronger scattering points are removed along with their neighborhood (strongest side lobes), Fig.8(a). The remaining part of the image is shown in Fig.8(b).

Example 5: Data based on the delta-wing experiment, described in [46], are considered in this example. The experiment was conducted by using an X-band radar operating at a center frequency of 10.1 GHz with 300 MHz bandwidth and a range resolution of 0.5 m. Three sets of data are analyzed in this example. Two sets are from the experiment simulator, while the third set are measured data. The pulse repetition time is $Tr = 1/2000 = 0.5$ ms. The total data set used in this example contains samples for 2048 range profiles with 50 bins. The target was a delta-wing shaped apparatus. It consisted of six-scatterer model. The target model has a length of 5 m on each of its three sides of regular triangle. The delta-wing is at a range of 2 km and was rotating at $3\,^{\circ}$/s. The nonlinear rotation with a maximal 1°/s. deviation in the rotation speed is superimposed. The range and the cross-range resolutions are $R_{\text{range}} = c/(2B) = 0.5\,\text{m}$, and $R_{\text{cross-range}} =$

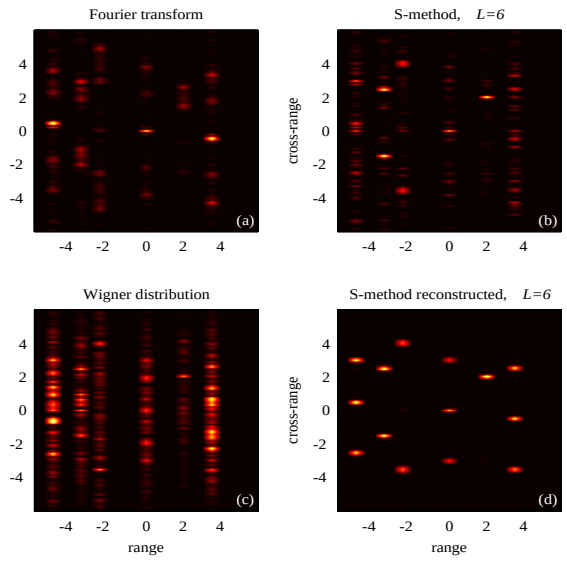

Fig. 7. The ISAR image based on: (a) The two-dimensional Fourier transform. (b) The S-method with $L = 6$. (c) The Wigner distribution. (d) The S-method based on the reconstructed signal in two steps ($s = 2$). Only 50% of randomly positioned available data are used in the reconstruction.

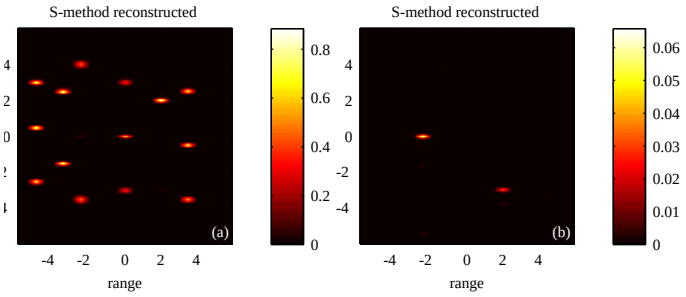

Fig. 8. (a) Reconstructed normalized image with colorbar values. (b) The same image after 14 the most significant scattering points are removed (detected and zero-valued) along with their surrounding side-lobes.

$\pi c/(\Omega_0 T_c \Omega_R) = 0.2770\,\mathrm{m}$ (calculated neglecting effects of the nonlinear rotation). The ISAR images obtained using the data without and with nonuniform motion are shown in Fig.9. Data within the interval of 50 range bins (where the target was located) are shown only. Image in actual range and cross-range values in meters is presented in the last figure. Data in Fig.9(a)-(f) correspond to the case when the nonlinear motion is not superimposed. Then there is no significant velocity nonlinearities and the FT based analysis produces satisfactory results. In the second case, when nonlinear motion is included, Fig.9(g)-(j), these nonlinearities make the FT based ISAR image unreadable. The S-method in this case improves the presentation and enables clear 6 point target identification. Images calculated based on full data set, Fig.9(a), are shown in left column of Fig.9. Images obtained from a reduced data set of 12.5% of the signal values, Fig.9(b), are presented in right column in Fig.9.

Results based on the measured data from this experiment are presented in Fig.9(k)-(n). The full set data based images are shown in Fig.9(k) and (m), while the results with unavailable samples are presented in Fig.9(l) and (n), for the FT based image and the S-method based image, respectively. The measured delta-wing data set was collected using $T_r = 1/2000$ s. Each range profile is generated in 0.5 ms and each profile had 41 bins. The total data set contains 60000 samples. The delta-wing was at a range of 2 km and was rotating at 2 $^{\circ}$/s. Only the data corresponding to the interval of 61 range bins (there the target was located) are used for calculation and presentation in Fig.9(k)-(n).

In order to illustrate influence of the assumed number of components K in the case of a direct reconstruction, with the FT (Section III) the calculations for data from Fig.9(a)-(f) are repeated with $K = 3$, $K = 9$, $K = 12$, $K = 24$, $K = 96$ and $K = 256$. They are shown in Fig.10. For too small value of $K = 3$ some of the scattering points are not reconstructed. This can easily be detected by calculating the MSE using available signal positions. equation (15).

A random position of the available samples has been assumed in Fig.9(b). Another possible scenario is that data blocks of a random duration are unavailable/corrupted, like in Fig.11(b). The reconstruction results in this case are presented in Fig.11(d). The results are similar to the case of random missing data as far as the randomness of data used in initial calculation is present in at least one direction, in order to provide random structure of variable in (6).

VI. Conclusion

An analysis of the ISAR image reconstruction in the case of a large number of unavailable or heavily corrupted data is presented. A simple method that can produce reconstruction in the case of uniform motion is reviewed, along with a simple an accurate analysis of the noise influence to the results. In the case of fast and complex target manoeuvring the ISAR image is blurred and the sparsity property is lost. For a large number of scattering points a parametric approach to refocus the image and reconstruct the signal with large number of missing data would be computationally extensive. A simple nonparametric method is used here to refocus image. Since it belongs to the class of quadratic time-frequency representations, a direct linear relation between the sparsity domain and the signal can not be established. Thus, the reconstruction task is appropriately reformulated. An adapted form of gradient algorithm is used to recover the ISAR image of the quality as in the case if all data were available. The efficiency of the proposed methods is illustrated on several numerical examples.

References

[1] V. C. Chen, H. Ling, "Time-frequency transforms for radar imaging and signal analysis", *Artech House*, Boston, USA, 2002.

[2] X. Bai, F. Zhou, M. Xing, Z. Bao, "High-resolution radar imaging of air-targets from sparse azimuth data", *IEEE Trans. Aerospace and Electronic Systems*, Apr. 2012, vol. 48, no. 2, pp. 1643-1655.

[3] L. Stanković, M. Daković, and T. Thayaparan, "Time-Frequency Signal Analysis with Applications", *Artech House*, Boston, March 2013

[4] F. Totir and E. Radoi, "Superresolution algorithms for spatial extended scattering centers," *Digital Signal Processing*, Vol. 19, No. 5, pp.780-792, Sept. 2009.

[5] M. Martorella and F. Berizzi, "Time windowing for highly focused ISAR image reconstruction," *IEEE Trans. Aerospace and Electronic Systems*, Vol. 41, No. 3, pp. 992–1007, 2005.

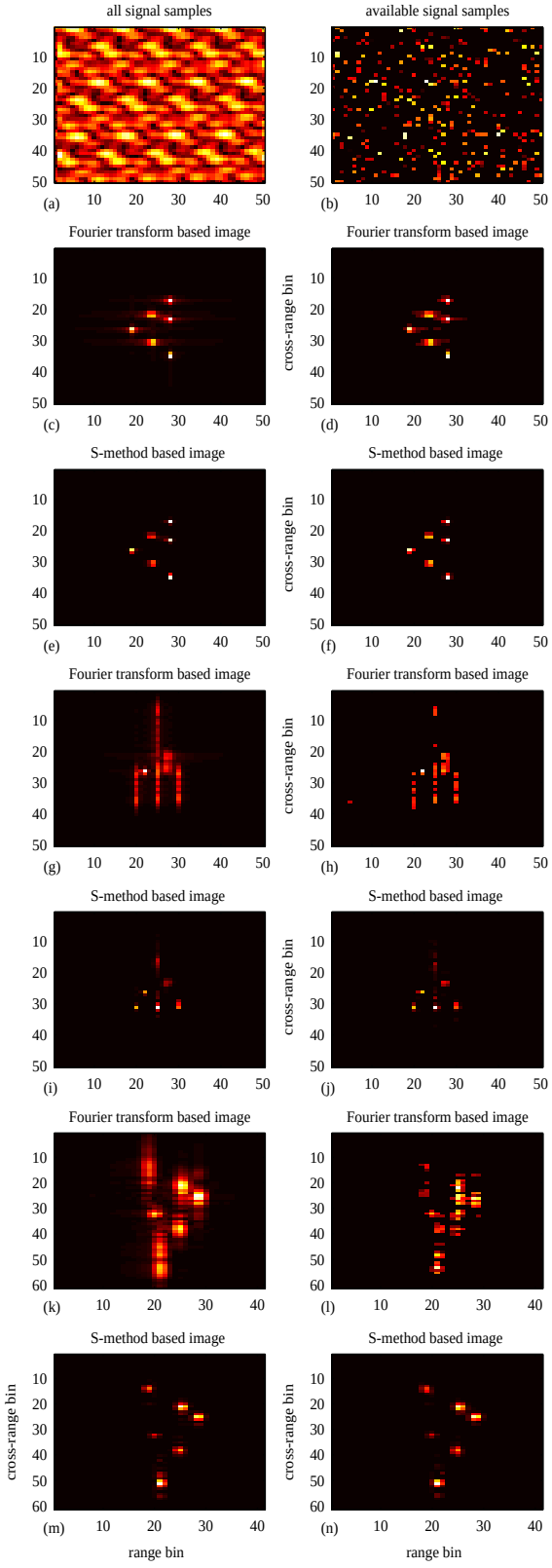

Fig. 9. The delta-wing experiment data: Full data are in the first column and the analysis based on 12.5% of the signal samples is in the second column. (a) All signal samples. (b) Available signal samples (unavailable samples are in black). (c)-(f) Images with the STFT and the S-method with full data set (left) and a reduced set of data (right) for a case when the motion is almost uniform. (g)-(j) Images with the STFT and the S-method with full data set (left) and a reduced sets of data (right) for the case when the motion for most of the scattering points is nonuniform. (k)-(l) Images with measured data set. The STFT and the S-method with full data set (left) and with a reduced set of data (right).

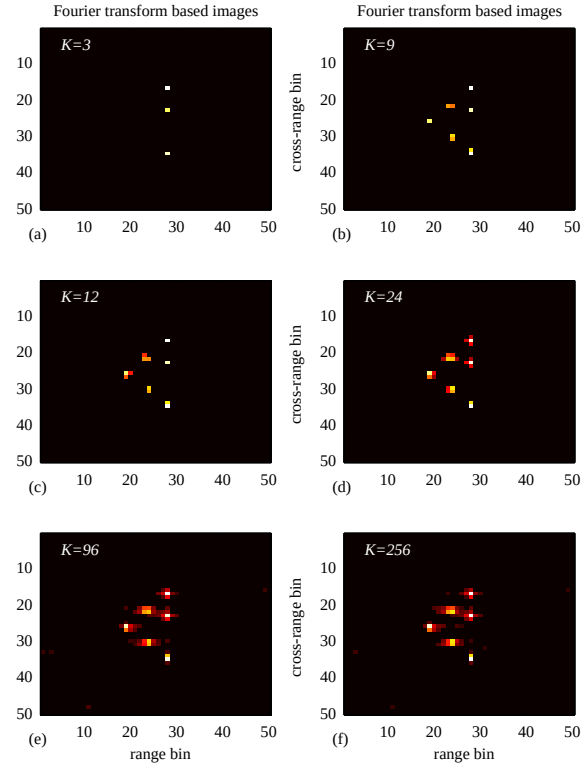

Fig. 10. Influence of the assumed number of components K to the analysis and reconstruction of radar data of a 6-point scatterer based on 12.5% of the signal samples.

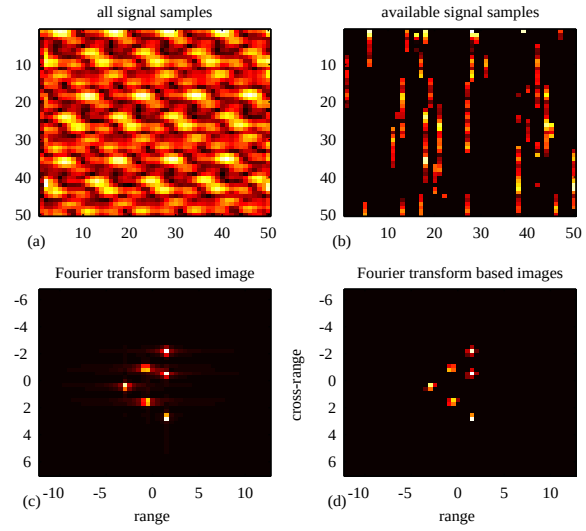

Fig. 11. Analysis of radar data of 6-point scatterer based on 12.5% of the signal samples missing in blocks. In the reconstruction $K = 30$ is used.

[6] M. Martorella, "Novel approach for ISAR image cross-range scaling," *IEEE Trans. Aerospace and Electronic Systems*, Vol. 44, No. 1, pp. 281–294, 2008.

[7] D. L. Donoho, "Compressed sensing," *IEEE Trans. Information Theory*, vol. 52, no. 4, pp. 1289–1306, 2006.

[8] E. J. Candès, J. Romberg, and T. Tao, "Robust uncertainty principles: Exact signal reconstruction from highly incomplete frequency information," *IEEE Trans. Information Theory*, vol. 52, no.2, pp. 489–509, 2006.

[9] S. G. Mallat and Z. Zhang, "Matching pursuits with time-frequency

dictionaries," *Signal Processing, IEEE Trans.*, vol. 41, no. 12, pp. 3397–3415, 1993.

[10] M. Wakin, S. Becker, E. Nakamura, M. Grant, E. Sovero, D. Ching, Y. Juhwan, J. Romberg, A. Emami-Neyestanak, E. Candes, "A Nonuniform Sampler for Wideband Spectrally-Sparse Environments," *Emerging and Selected Topics in Circuits and Systems, IEEE Journal on*, vol.2, no.3, pp.516,529, Sept. 2012.

[11] M. Mishali,Y.C. Eldar, "From Theory to Practice: Sub-Nyquist Sampling of Sparse Wideband Analog Signals," *Selected Topics in Signal Processing, IEEE Journal of*, vol.4, no.2, pp.375,391, April 2010.

[12] R. Grigoryan, T. L. Jensen, T. Arildsen, T. Larsen, "Reducing the computational complexity of reconstruction in compressed sensing nonuniform sampling," in *Proceedings of the 21st EUSIPCO 2013*, Sept. 2013.

[13] J. A. Tropp, J.N. Laska, M.F. Duarte, J.K. Romberg, R.G. Baraniuk, "Beyond Nyquist: Efficient Sampling of Sparse Bandlimited Signals," *Information Theory, IEEE Transactions on*, vol.56, no.1, pp.520,544, Jan. 2010.

[14] D. Needell and J. A. Tropp, "CoSaMP: Iterative signal recovery from incomplete and inaccurate samples," *Applied and Computational Harmonic Analysis*, vol. 20, no. 3, pp. 301–321,2009

[15] L. Stanković, S. Stanković, I. Orović, and M. Amin, "Robust Time-Frequency Analysis based on the L-estimation and Compressed sensing," *IEEE Signal Processing Letters*, Vol. 20, No. 5, pp. 499-502.

[16] M. A. Figueiredo, R. D. Nowak, and S. J. Wright, "Gradient projection for sparse reconstruction: Application to compressed sensing and other inverse problems,"*IEEE Journal of Selected Topics in Signal Processing*, vol. 1, no. 4, pp. 586–597, 2007.

[17] L. Stanković, M. Daković, and S. Vujović, "Adaptive Variable Step Algorithm for Missing Samples Recovery in Sparse Signals," *IET Signal Processing*, Volume 8 , no. 3, May 2014, pp.246-256.

[18] J. H. G. Ender, "On compressive sensing applied to radar," *Signal Processing*, Vol. 90, No. 5, 1402-1414, 2010.

[19] X. Zhang; Ting Bai; Hongyun Meng; Jiawei Chen, "Compressive Sensing-Based ISAR Imaging via the Combination of the Sparsity and Nonlocal Total Variation," *Geoscience and Remote Sensing Letters, IEEE* , vol.11, no.5, pp.990,994, May 2014

[20] R.G Raj, M. Farshchian, "ISAR imaging in sea clutter via compressive sensing," *Waveform Diversity and Design Conference (WDD), 2010 International* , vol., no., pp.200,205, 8-13 Aug. 2010

[21] S. Chai, W. Chen, and C. Chen, "Sparse Fusion Imaging for a Moving Target in T/R-R Configuration", *Sensors*, Jun 2014, 10664–10679.

[22] L. Stanković, M. Daković, T. Thayaparan, and V. Popović-Bugarin, "Signal Decomposition of Micro-Doppler Signatures," *Radar Micro-Doppler Signatures: Processing and Applications*, Ed. V. C. Chen, D. Tahmoush, and W. J. Miceli, IET, pp.273-327, 2014

[23] W. Rao, G. Li, X. Wang, X.-G. Xia, "Parametric sparse representation method for ISAR imaging of rotating targets," *IEEE Trans. Aerospace and Electronic Systems*, vol.50, no.2, pp.910,919, April 2014

[24] S.J. Wu, L. Zhang; M.D. Xing, "Super-resolution ISAR imaging via statistical compressive sensing," Radar (Radar), 2011 *IEEE CIE International Conference* on , vol.1, no., pp.545,550, 24-27 Oct. 2011.

[25] S.B. Peng, J. Xu, Y.N. Peng, J.B. Xiang, "Parametric inverse synthetic aperture radar maneuvering target motion compensation based on particle swarm optimizer," *IET Radar Sonar Navigat.* 5, 305–314 (2011).

[26] J.H. Park and N.H. Myung, "Enhanced and efficient ISAR image focusing using the discrete Gabor representation in an oversampling scheme," *Progress In Electromagnetics Res.*, Vol.138, 227-244, 2013.

[27] L. Stanković, M. Daković, T. Thayaparan, and V. Popović-Bugarin, "Micro-Doppler Removal in the Radar Imaging Analysis," *IEEE Trans. Aerospace and Electronic Systems*, Vol.49, April 2013, pp.1234-1250.

[28] Shin, S. Y. and N. H. Myung, "The application of motion compensation of ISAR image for a moving target in radar target recognition," *Microwave and Optical Technology Lett.*, Vol.50, No. 6, 1673-1678, 2008.

[29] I. Djurovic, T. Thayaparan, L. Stankovic, "Adaptive Local Polynomial Fourier Transform in ISAR", *EURASIP Journal on Applied Signal Processing*, Vol. 2006, Article ID 36093, 2006.

[30] L. Xiumei, B. Guoan, J. Yingtuo, "Quantitative SNR Analysis for ISAR Imaging using LPFT," *IEEE Trans. Aerospace and Electronic Systems*, vol.45, no.3, pp.1241,1248, July 2009

[31] L. Stankovic, T. Thayaparan, V. Popovic, I. Djurovic, M. Dakovic, "Adaptive S-Method for SAR/ISAR Imaging", *EURASIP Journal on Advances in Signal Processing*, Vol. 2008.

[32] Y. Wang and Y.-C. Jiang: "ISAR imaging of ship target with complex motion based on new approach of parameters estimation for polynomial phase signal," *EURASIP Journal on Advances in Signal Processing*, Vol. 2011 (2011), Article ID 425203, 9 pages.

[33] F Berizzi, M Martorella, A Cacciamano, A Capria, "A contrast-based algorithm for synthetic range-profile motion compensation," *IEEE Trans. Geosci. Remote Sens. 4*6, 3053–3062 (2008)..

[34] Y. Wang, H. Ling, and V. C. Chen, "ISAR motion compensation via adaptive joint time-frequency techniques," *IEEE Trans. Aerospace and Electronic Systems*, Vol. 38, No. 2, pp. 670-677, 1998.

[35] Y. Li, M. Xing, J. Su, Y. Quan, Z. Bao, "A New Algorithm of ISAR Imaging for Maneuvering Targets with Low SNR," *IEEE Trans. Aerospace and Electronic Systems* , vol.49, no.1, pp.543,557, Jan. 2013

[36] L. Stanković, "A method for time-frequency signal analysis," *IEEE Transactions on Signal Processing*, Vol-42, No.1, Jan.1994.pp.225-229.

[37] L. Stanković, S. Stanković, and M. Daković, "From the STFT to the Wigner distribution," *IEEE Signal Processing Magazine*, Vol. 31, No. 3, May 2014, pp. 163-174 (www.tfsa.ac.me/LN).

[38] A. G. Stove, "Linear FMCW radar techniques," Radar and Signal Processing, IEE Proceedings F , vol.139, no.5, pp.343,350, Oct. 1992.

[39] J.M. Munoz-Ferreras, F. Perez-Martinez, "On the Doppler Spreading Effect for the Range-Instantaneous-Doppler Technique in Inverse Synthetic Aperture Radar Imagery," *Geoscience and Remote Sensing Letters, IEEE*, vol.7, no.1, pp.180,184, Jan. 2010

[40] L. Stanković, S. Stanković, and M. G. Amin, "Missing Samples Analysis in Signals for Applications to L-Estimation and Compressive Sensing", *Signal Processing*, Vol.94, Jan.2014, pp.401–408.

[41] S. Stanković, I. Orović, and L. Stanković, "An Automated Signal Reconstruction Method based on Analysis of Compressive Sensed Signals in Noisy Environment", *Signal Processing*, Vol.104, Nov.2014, pp.43–50.

[42] L. Stanković, "A measure of some time–frequency distributions concentration", *Signal Processing*, Vol. 81, No. 3, pp. 621-631, March 2001.

[43] L. Stankovic, M Dakovic, "Reconstruction of Randomly Sampled Sparse Signals Using an Adaptive Gradient Algorithm", *Sig. Proc.*, submitted (http://arxiv.org/pdf/1412.0624v1.pdf).

[44] M.A. Sustika, J.A. Tropp, I.S. Dhillona, R.W. Heath Jr., On the existence of equiangular tight frames, *Linear Algebra and its Applications*, Vol.426, no. 2–3, Oct. 2007, pp.619–635.

[45] M Dakovic, L. Stankovic, S. Stankovic, "Gradient Algorithm Based ISAR Image Reconstruction From the Incomplete Dataset", *Int. Conf. CoSeRa*, 2015.

[46] T. Thayaparan, L. Stankovic, C. Wernik, M Dakovic, "Real-time motion compensation, image formation and image enhancement of moving targets in ISAR and SAR using S-method based approach," *Signal Processing, IET* , vol.2, no.3, pp.247,264, Sept. 2008.

Ljubiša Stanković (*M'91–SM'96–F'12*) was born in Montenegro in 1960. He received the B.S. degree in EE from the University of Montenegro (UoM), the M.S. degree in Communications from the University of Belgrade and the Ph.D. in Theory of Electromagnetic Waves from the UoM. As a Fulbright grantee, he spent 1984-1985 academic year at the Worcester Polytechnic Institute, USA. Since 1982, he has been on the faculty at the UoM, where he has been a full professor since 1995. In 1997-1999, he was on leave at the Ruhr University Bochum, Germany, supported by the AvH Foundation. At the beginning of 2001, he was at the Technische Universiteit Eindhoven, The Netherlands, as a visiting professor. He was vice-president of Montenegro 1989-90. During the period of 2003-2008, he was Rector of the UoM. He was Ambassador of Montenegro to the UK, Ireland, and Iceland from 2010 to 2015. His current interests are in Signal Processing. He published about 370 technical papers, more than 130 of them in the leading journals, mainly the IEEE editions. Prof. Stanković received the highest state award of Montenegro in 1997, for scientific achievements. He was a member the IEEE SPS Technical Committee on Theory and Methods, an Associate Editor of the *IEEE Transactions on Image Processing*, the *IEEE Signal Processing Letters*, *IEEE Transactions on Signal Processing*, and numerous special issues of journals. Prof. Stanković is a member of Editorial Board of *Signal Processing*. He is a member of the National Academy of Science and Arts of Montenegro (CANU) since 1996 and a member of the European Academy of Sciences and Arts.